A methodology to assess the effects of biofilm roughness on substrate fluxes using image analysis, substrate profiling, and mathematical modelling

J. P. Pavissich, M. Aybar, K. J. Martin and R. Nerenberg

ABSTRACT

We present a novel approach, based on image analysis and modelling, to study the impact of morphological variability (roughness) and fluid dynamics on substrate mass fluxes in biofilms. Specifically, we used this method to assess substrate fluxes in counter-diffusional autotrophic biofilms in a hydrogen-based membrane biofilm reactor. The physical structure of the biofilm was determined *in situ* at the meso-scale using stereomicroscopy. Image analysis was used to characterize the biofilm structure, and substrate profiles were obtained using microsensors. A two-dimensional, continuum biofilm model including microbial reactions, mass transport, and fluid dynamics was developed to compute substrate conversion in irregularly shaped counter-diffusional biofilms. Experimental biofilm structures were reproduced in the model and simulated under the prevailing substrate and hydrodynamic conditions for flow velocities varied over three orders of magnitude. Model calculations were consistent with experimental results and showed enhanced conversion rates with increased roughness at higher flow velocities. Also, modelling showed that conversion rates in counter-diffusional biofilms were typically higher than in co-diffusional biofilms. This study highlights the potential to use a simple image acquisition approach coupled to a theoretical model, to evaluate biofilm overall substrate utilization related to biofilm morphological heterogeneity.

Key words | biofilm model, counter-diffusion, image analysis, membrane biofilm reactor (MBfR), substrate conversion

J. P. Pavissich
M. Aybar
K. J. Martin
R. Nerenberg (corresponding author)
Department of Civil and Environmental Engineering and Earth Sciences,
University of Notre Dame,
Notre Dame,
IN 46556,
USA
E-mail: *rnerenbe@nd.edu*

INTRODUCTION

Biofilms may assume diverse surface morphologies, ranging from smooth to rough. Biofilm morphological heterogeneity (roughness) can lead to significant effects on substrate conversion rates due to mass transport limitations subject to the hydrodynamic and substrate availability conditions. Past research has shown, via modelling, that biofilms with different degrees of roughness or substratum coverage can have very different average mass fluxes of growth substrates (Rittmann *et al.* 1999; Eberl *et al.* 2000; Picioreanu *et al.* 2000). While most research has addressed substrate transformation in conventional biofilms, few studies have addressed counter-diffusional biofilms (Semmens & Essila 2001; Terada *et al.* 2007), where one growth substrate (either electron donor or acceptor) enters the biofilm from the bulk fluid, while the other is delivered from the base of the biofilm. Also, most studies addressing the effects of roughness on substrate conversion are based on modelling, and lack experimental validation.

Counter-diffusional biofilms are ubiquitous in nature and relevant in biotechnological water purification applications, such as membrane biofilm reactors (MBfRs) (Martin & Nerenberg 2012). Counter-diffusional biofilms can behave quite differently from conventional, co-diffusional biofilms because the mass transfer boundary layer helps to retain the substrate entering the biofilm from the attachment surface and a high microbial activity can be maintained in the inner biofilm portions (Martin & Nerenberg 2012). Also, local thickness variation and incomplete substratum coverage may increase fluxes by increasing exposure to substrates (Martin *et al.* 2013). No previous

doi: 10.2166/wst.2014.103

research has addressed the effects of structural heterogeneity on counter-diffusional biofilms substrate conversion. A systematic study is needed.

Currently, the study of the physical structure of biofilms typically include the use of compound light and confocal-laser scanning microscopy (CLSM) coupled to image analysis (Heydorn *et al.* 2000; Yang *et al.* 2000). The use of microscopy allows working with intact biofilms, but addresses structure mainly at the micro-scale. It also may require invasive biofilm manipulation prior to analysis, e.g., *ex situ* preparation, fixation, hybridization.

The main objective of this study was to develop a combined experimental and modelling approach to study substrate conversion rates in rough biofilms. We focused our study on a membrane-attached biofilm growing on a MBfR. In MBfRs, the prediction of biofilm conversion rates from substrate fluxes requires the determination of biofilm heterogeneity (Wanner *et al.* 2006). One-dimensional models have been widely used for studying counter-diffusion and microbial ecology in MBfRs (Terada *et al.* 2007; Downing & Nerenberg 2008a). However, multidimensional modelling is needed for accurate representation of morphological heterogeneity. Substrate conversion was estimated in an experimental MBfR and a two-dimensional (2D) continuum model was used to simulate the membrane-attached biofilm. Substrate mass fluxes and conversion rates were computed in the model under laminar fluid flow and including also conventional substrate co-diffusion. The model predictions were then validated by comparing the simulations with the experimental results for an identical biofilm structure. A novel aspect of this research was the simulation of a real experimental biofilm structures model obtained with a relatively simple and non-destructive imaging approach with a high resolution potential.

METHODS

Membrane biofilm reactor configuration

A column MBfR with a single hollow-fibre membrane (HFM) was built. The reactor consisted of a 0.6 cm side, square-section glass tube, 18 cm in length, with two 0.4 cm inner diameter ports along its length (Figure 1). An 18 cm long composite, microporous polyethylene HFM with a dense polyurethane core (HFM200TL, Mitsubishi Rayon, Japan), with a 280 μm inside diameter (Ahmed *et al.* 2004), was placed in the centre of the tube, allowing uniform flow in the column and uniform shear on the fibre. We have extensively used this experimental set-up for studying MBfRs (Downing & Nerenberg 2008a, b). Glass cover slips embedded in the reactor walls supported microscopy analysis. The ports were used for microsensor measurements in the biofilm (see below). A short hydraulic retention time of 32 min, calculated using the combined reactor and tubing volume, prevented the accumulation of planktonic bacteria. A recirculation flow rate was used to ensure complete mixing and to apply different

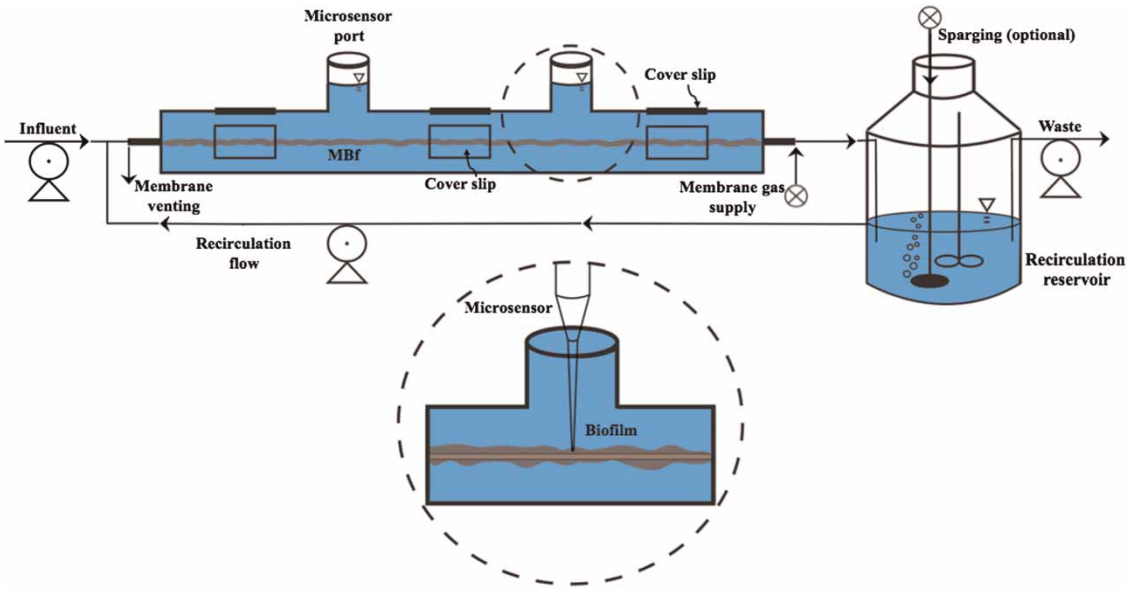

Figure 1 | Membrane biofilm reactor experimental set-up.

hydrodynamic conditions to the system. The HFM was pressurized with hydrogen gas and operated in dead end mode, but was vented on a daily basis to prevent accumulation of water condensate.

Biofilm experiments

A mineral medium (pH = 7.0) was used as reactor influent and consisted, per litre of ultra-pure water, of 1.386 g Na_2HPO_4, 0.849 g KH_2PO_4, 0.025 g $(NH_4)_2SO_4$, 0.05 g $MgSO_4 \cdot 7H_2O$, and 1 mL aliquots of Ca–Fe and trace element solutions (Downing & Nerenberg 2008a). The reactor was fed with influent at 0.5 mL/min supplied with a dissolved oxygen concentration of approximately 7 mg/L and the HFM with an intra-membrane hydrogen pressure of 14 kPa. The system was inoculated with fresh activated sludge from a local municipal treatment plant and operated in batch mode for 2 days to promote biofilm establishment at a recirculation flow rate of 2 mL/min. After inoculation the reactor was operated in continuous mode with a 25 mL/min recirculation rate. After 21 days of operation, a pseudo steady-state biofilm was reached, where biofilm average thickness was constant over time along a representative section of membrane. The biofilm was characterized using hydrogen and oxygen microsensors and microscopy (see below). The substrate conversion of the membrane-attached biofilm was evaluated under different hydrodynamic conditions. The flow rates were 2, 10, 50 and 200 mL/min, providing average flow velocity values of 0.001, 0.005, 0.025 and 0.1 m/s. Hydrogen was the electron donor and oxygen the acceptor, allowing substrate profiles to be determined using commercially available microsensors. The experiments were conducted at room temperature (22 °C).

Biofilm substrate flux measurements

Clark-type microelectrodes with respective tip diameters of 10 and 25 μm (Unisense A/S, Aarhus, Denmark) were used to measure dissolved oxygen and hydrogen concentrations in the biofilm. Measurements were taken at spatial intervals of 25 μm through the biofilm depth. The sensors were positioned and moved with a micromanipulator (MM32-2, Unisense A/S, Aarhus, Denmark). Five sets of substrate profiles were collected in triplicate for each sampling port. The length of membrane assessed for each port was 0.2–0.4 cm. The biofilm was relatively homogeneous in average thickness along the membrane for each experiment. Oxygen mass fluxes ($g/(m^2 \cdot d)$) into the biofilm were calculated from microprofile measurements across the mass boundary layer, as previously described, using Fick's first law (Downing & Nerenberg 2008b).

Microscopy and image analysis

For imaging the membrane-attached biofilm, we used a stereo-zoom light microscope (Cole-Palmer, Chicago, IL) equipped with a mounted digital camera (Cybershot DSC-F707, Sony) and a fibre-optic light source. The camera was fixed to the microscope with a ×1 mounting adapter. The intensity and angle of incidence of the light source was regulated to achieve higher contrast between the biofilm, membrane and background. Image acquisition was done *in situ* on the MBfR. Samples were viewed using a ×2 objective with a numerical aperture (NA) of 0.06 and a ×4 objective with 0.1 NA, and the camera ×10 optical zoom for an overall magnification of ×20 and ×40. The minimum detectable characteristic length for this set-up, estimated by the Rayleigh criterion, is 6.0 and 3.6 μm, respectively (Milferstedt *et al*. 2009). The camera has a resolution of 4.9 Mega pixels (1,920 × 2,560 pixels), and we obtained a conversion factor of 2.0 and 1.0 μm/pixel for the ×20 and ×40 magnification. These microscope and camera specifications allow for the determination of very thin biofilms. The system was used to obtain images for a membrane length of 0.25–0.5 cm. Images were processed for analysis based on a methodology adapted from previous work (Lewandowski & Beyenal 2007). Specifically, the images were taken using a perpendicular reference to the objective (Figure 2). Image analysis software was developed using MATLAB (Mathworks, Natick, Massachusetts, USA). The analysis consisted of the following steps: pixel detection of membrane–biofilm and biofilm–liquid interfaces, conversion from RGB to a binary image, and calculation of biofilm physical parameters. Through biofilm pixel identification and counting, the biofilm height on the image abscissa was measured automatically, and a high-resolution matrix containing spatial coordinates in pixels for the biofilm surface was generated. The biofilm projected area, perimeter and roughness for each previously substrate profiled membrane sample were calculated as shown before (Picioreanu *et al*. 2000; Lewandowski & Beyenal 2007). Pixels were transformed to μm using a standard eyepiece micrometre scale and the membrane diameter as reference.

Biofilm model description

Structural heterogeneity in biofilms can lead to important multi-dimensional components of substrate fluxes (De Beer

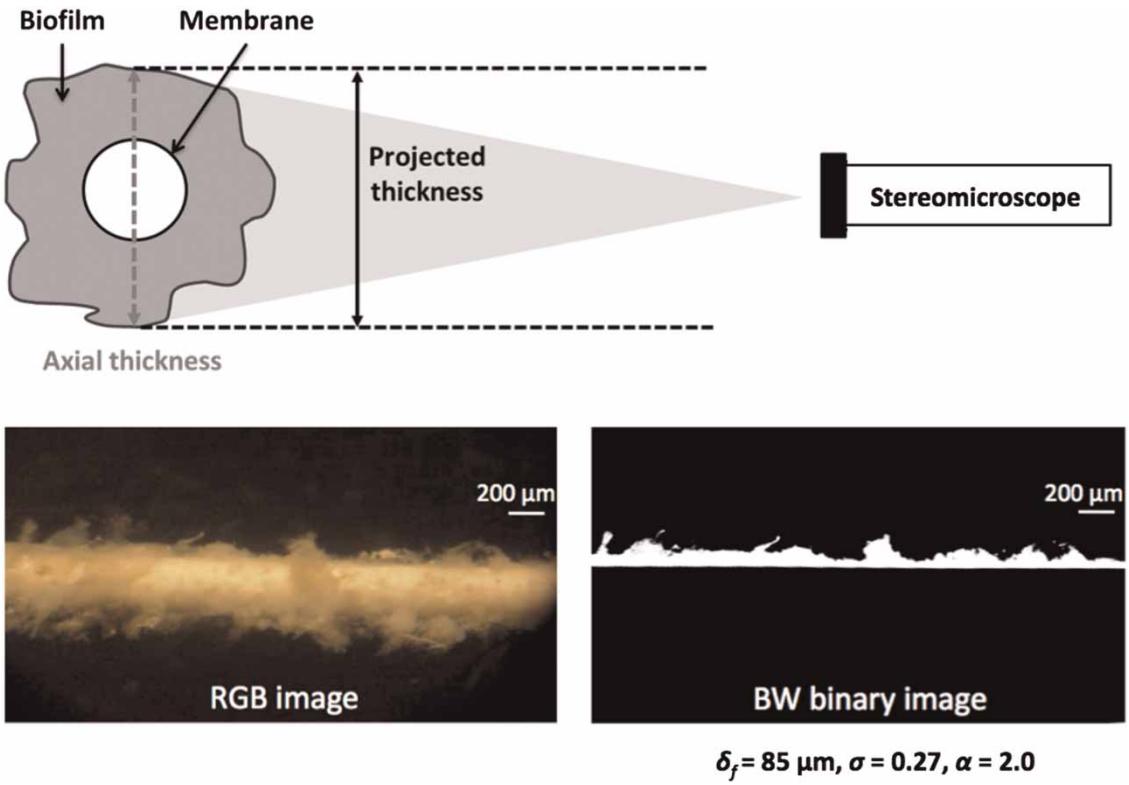

Figure 2 | Image acquisition and processing scheme. The binary image (bottom right) represents the biofilm on the top of the membrane (bottom left). Structural parameters are shown.

et al. 1994). A 2D continuum biofilm model was chosen based on the good agreement found between this approach and three-dimensional (3D) biofilm simulations for analysing substrate mass transfer and conversion rates in continuous systems (Eberl *et al.* 2000; Picioreanu *et al.* 2000). An extra dimension did not introduce significant differences for a qualitative analysis, but added considerable computational effort. This has been also shown in particle-based and hybrid biofilm models (Alpkvist *et al.* 2006).

The spatial 2D modelling domain consisted of a rectangular $L_X \times L_Y$ channel representing an MBfR section. The system included a solid biofilm subdomain, Ω_B, and a bulk liquid subdomain, Ω_L, with soluble substrates. The compartments were separated by an interface Γ_{LB}. The biofilm was attached to the bottom boundary Γ_M, which represents the surface of a gas-transferring membrane. For studying counter-diffusion, a flux of gaseous substrate into the system was designated (Figure 3).

From the biofilm geometry, biofilm average thickness (δ_f) and dimensionless parameters were calculated. These included surface relative roughness (σ) and area enlargement (α) (Picioreanu *et al.* 2000). The model was used to simulate the experimental aerobic autotrophic MBfR biofilm with hydrogen supplied by the membrane and dissolved oxygen contained in the bulk liquid (counter-diffusion). The data obtained using image analysis were used to reproduce the biofilm structures in MATLAB. The image analysis structural parameters were also validated with the model calculations. Fluid dynamics and mass transport were computed in Ω_L considering laminar flow between two parallel plates with an average velocity u and a fully developed velocity profile assigned at the inlet boundary (Figure 3). The outlet boundary had a reference pressure of zero, and no-slip wall conditions were assigned at the outermost surface of the flow channel and biofilm surface. The system was modelled assuming an axial symmetry, representing half of a parallel plate duct. This was because the membrane support had axial symmetry and the experimental substrate profiles were taken on the top half of the MBfR. To reduce the computational burden for solving fluid dynamics, half of the velocity profile was considered, assuming maximum velocity at the top boundary. A range of velocities was simulated, including those tested in the experiments and reported in biofilm reactors (Picioreanu *et al.* 2000). The Re number was calculated using

$$\mathrm{Re} = \frac{u}{\upsilon}(L_Y - \delta_f) \quad (1)$$

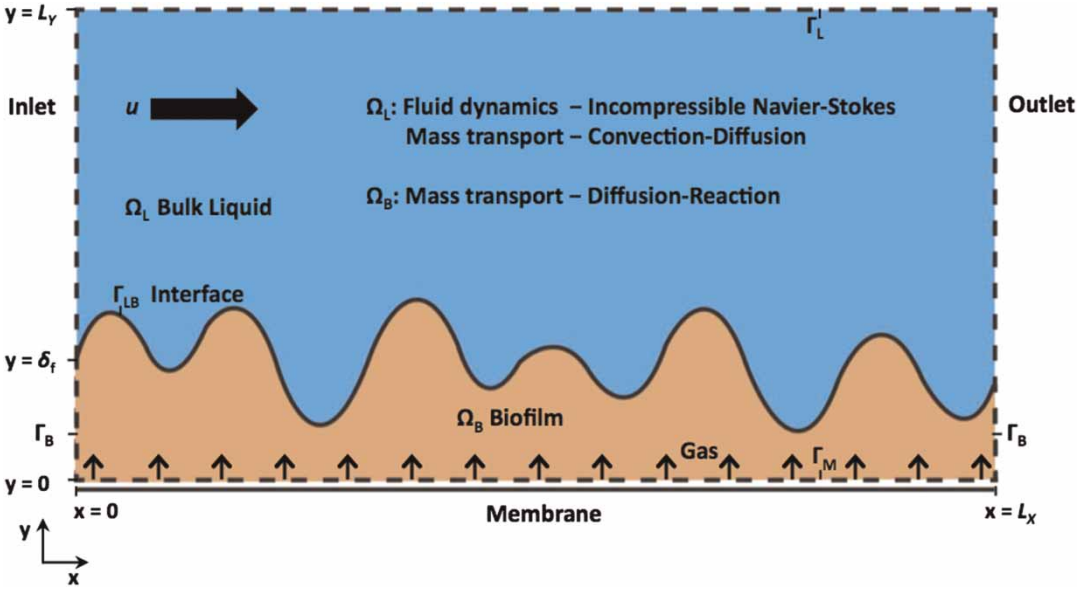

Figure 3 | Biofilm conceptual model description and domain.

where υ is the fluid kinematic viscosity (Table 1). Steady, laminar flow was assumed throughout the channel and modelled using the incompressible Navier–Stokes equations. Substrate transport by convection and diffusion were solved (Martin *et al.* 2013). In Ω_B, substrate transport was modelled considering only diffusion ($u = 0$) described by Fick's Law and assuming effective diffusion coefficients as presented elsewhere (Stewart 2003). Substrate reaction due to microbial consumption was included in the mass balances (Martin *et al.* 2013) and modelled by Monod kinetics (Bae & Rittmann 2000). Both electron donor and acceptor substrate limitation were considered in the rate equations. In Ω_L, no substrate uptake was assumed. For the substrates, the liquid outlet boundary was assigned a convective flux, and continuity was assumed at the liquid–biofilm interface. For all simulations, an inlet bulk liquid oxygen concentration of 7 g/m^3 and an intra-membrane hydrogen pressure of 14 kPa were used. The hydrogen flux J_{H_2} to the biofilm at the membrane boundary was assigned by

$$J_{H_2} = k_{mem}\left(\frac{p_{H_2}}{H_{H_2}} - S_{H_2}\right) \quad (2)$$

based on intra-membrane hydrogen partial pressure p_{H_2}, mass transfer coefficient across the membrane k_{mem}, hydrogen Henry's law coefficient H_{H_2}, and hydrogen concentration at the membrane surface S_{H_2}. The selected supply intra-membrane pressure resulted in a hydrogen concentration of approximately 1.5 g/m^3 at the biofilm base for all simulations. The model kinetic and physical parameters are summarized in Table 1.

Model solution

The model was solved for steady-state using the finite element solvers of the multiphysics software COMSOL 3.5a (Comsol Inc., Burlington, MA). The simulations were run on the University of Notre Dame Center for Research Computing computational grid using 12 to 32 GB RAM nodes.

Measures of biofilm performance were calculated from the model output. Total substrate conversion per projected substratum area (Φ), with mass flux units, was calculated integrating the total flux (J_n) over the biofilm surface at the liquid–biofilm interface and dividing by the membrane section length according to Equation (3):

$$\Phi = \frac{1}{L_X}\int_{\Gamma_b} J_n dA_{\Gamma_b} \quad (3)$$

The calculations were performed for the biofilm surface between $x = 100$ μm and $x = L_X - 100$ μm to minimize the inlet and outlet boundary effects. Substrate limitation and biological utilization according to Monod kinetics was evaluated using the non-dimensional relative microbial activity coefficient for the biofilm substrate concentrations, defined

Table 1 | Model and experimental parameters

Parameter	Symbol	Value	Unit	Reference
Domain dimensions	$L_X \times L_Y$	$2{,}500 \times 1{,}500$	μm	
Flow velocity	u	0.001; 0.005; 0.025; 0.1; 0.25	m/s	
Water kinematic viscosity	v	8.9×10^{-7}	m^2/s	at 25 °C
Re number	Re	1.7; 8.5; 42; 168; 420		
Influent oxygen concentration	S_{O_2}	7	g_{O_2}/m^3	
Intra-membrane hydrogen pressure	p_{H_2}	14	kPa	
Diffusivity of hydrogen in water	D_{H_2}	4.5×10^{-9}	m^2/s	Stewart (2003)
Diffusivity of oxygen in water	D_{O_2}	2.0×10^{-9}	m^2/s	Stewart (2003)
Diffusivity ratio biofilm/water	f	0.6		Stewart (2003)
Membrane gas mass transfer coefficient	k_{mem}	5×10^{-5}	m/s	Ahmed *et al.* (2004)
Henry's law coefficient for hydrogen	H_{H_2}	65	m^3·kPa/g	at 25 °C
Biofilm density	ρ_f	30	kg_{COD}/m^3	Martin *et al.* (2013)
Maximum rate of substrate utilization	q_{max}	1.33	$g_{H_2}/(g_{COD}$·d)	Rittmann & McCarty (2001)
Decay coefficient	b	0.05	1/d	Rittmann & McCarty (2001)
Half-saturation coefficient for oxygen	K_{O_2}	0.1	g_{O_2}/m^3	Picioreanu *et al.* (2000)
Half-saturation coefficient for hydrogen	K_{H_2}	0.008	g_{H_2}/m^3	Martin *et al.* (2013)
Biomass yield on hydrogen	Y	1.93	g_{COD}/g_{H_2}	Rittmann & McCarty (2001)

as the product of the Monod terms:

$$\text{Relative activity} = \frac{[S_{H_2}]}{K_{H_2} + [S_{H_2}]} \frac{[S_{O_2}]}{K_{O_2} + [S_{O_2}]} \quad (4)$$

with bacteria being fully substrate limited when the activity is 0 and achieving maximum utilization at an activity of 1 (Martin & Nerenberg 2012).

Model validation and application

Total substrate conversion rates and activity profiles obtained for the different experimental MBfR biofilm sections were compared to the numerical model results at the same experimental flow velocity values of 0.001, 0.005, 0.025 and 0.1 m/s. Also, we used the model to study the effect of roughness on substrate conversion comparing counter-diffusion to co-diffusion on the two sections with substantially different roughness values. We included an additional velocity of 0.25 m/s for these studies. Co-diffusion was simulated by imposing an impermeable wall at the membrane boundary and an inlet bulk liquid hydrogen concentration of 1.5 g/m^3.

RESULTS AND DISCUSSION

Membrane-attached biofilm characterization and activity

Experimental MBfR biofilm sections of 0.25 cm in length, at pseudo-steady state, were selected for image analysis and substrate flux determination. Similar average thickness and area enlargement parameters, and different roughness coefficients were found for the biofilm sections (Figures 2 and 4(a)). The roughness values were considered from moderate to very high (Picioreanu *et al.* 2000). The projected axial thickness of the biofilm (Figures 2 and 4(a)) is not an exact representation of the actual 3D biofilm. However, 2D approximations are often used by modellers and considered to be sufficiently good (Eberl *et al.* 2000). Using the experimental oxygen profiles (Figures 4(c) and 4(d)), we determined the substrate fluxes into the biofilm for different flow velocities. Oxygen conversion rates per projected membrane area were also calculated (Figure 5). Average oxygen fluxes showed an increase in substrate conversion with higher flow velocities. Concentration profiles for lower flow velocities showed more oxygen limitation

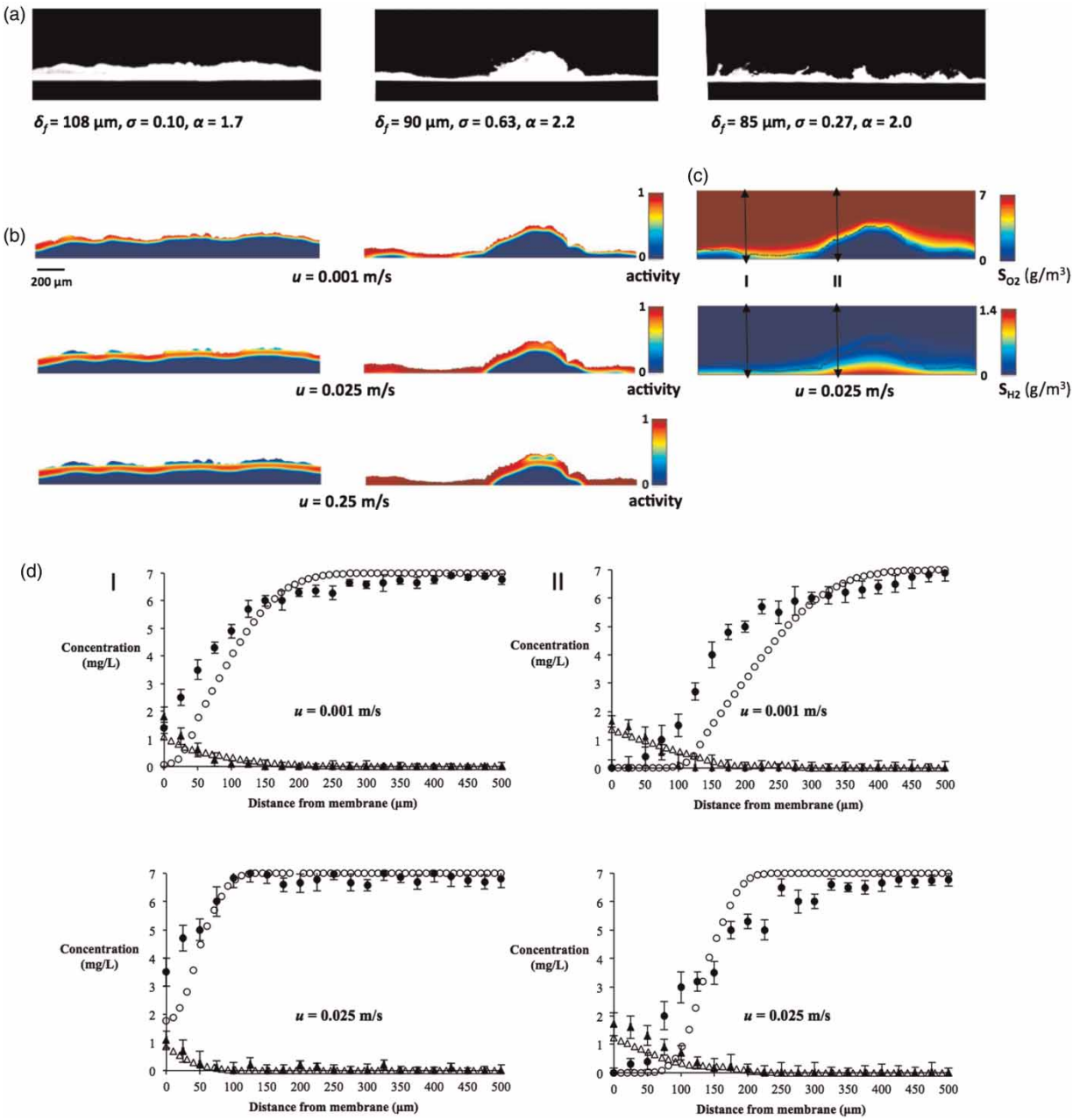

Figure 4 | Characterization of counter-diffusional biofilms. (a) Acquired images and their structural parameters. (b) Modelled biological activity profiles for the biofilm sections, $u = 0.001$, 0.025 and 0.25 m/s. (c) Simulated oxygen and hydrogen concentrations for the second biofilm illustrating substrate counter-diffusion, $u = 0.025$ m/s. (d) Oxygen and hydrogen concentration profiles at points I and II shown in (c), $u = 0.001$ and 0.025 m/s, ○ = S_{O2} (model); ● = S_{O2} (experimental); △ = S_{H2} (model); ▲ = S_{H2} (experimental).

within the biofilm and thus a lower overall activity (Figures 4(b)–4(d)).

The use of stereomicroscopy imaging, coupled to modelling and substrate profiling, provides a simple and non-destructive system to address biofilm structural parameters and substrate uptake at the meso-scale, with no need for further biofilm manipulation. Stereomicroscopy uses reflected light instead of transmitted light, allowing examination of specimens that would be too thick or opaque for conventional light microscopy. Another non-destructive and relatively easy-to-perform technique for measuring biofilm thicknesses *in situ* has been described for membrane-attached systems elsewhere (Dos Santos & Livingston 1995). Here, the image of a membrane with attached biofilm is projected onto a screen with an attached scale and the image projection is recorded. The thickness of

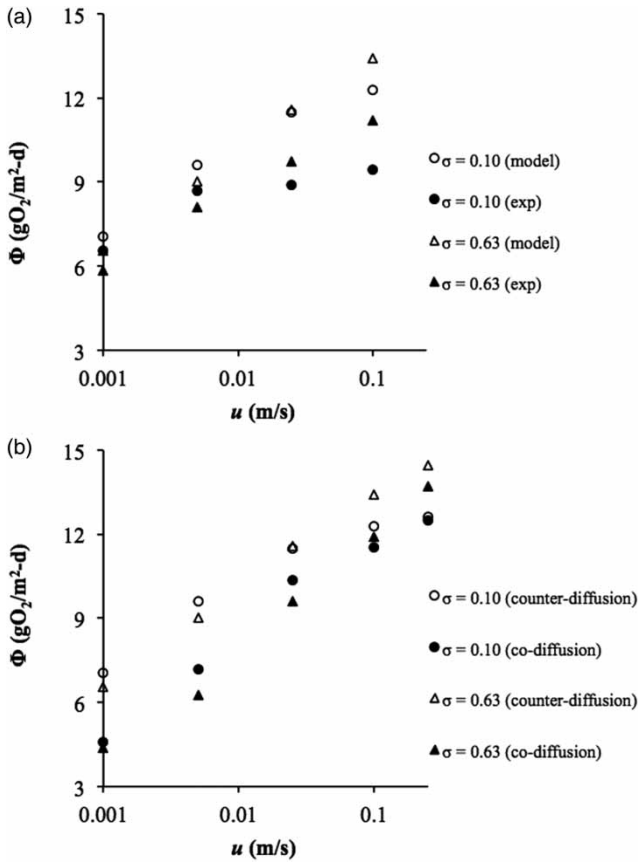

Figure 5 | Total substrate conversion rates per projected area for counter- and co-diffusional biofilms, as a function of flow velocity, for the biofilm sections shown in Figure 4. (a) Experimental and modelling results (counter-diffusion). (b) Modelling results (counter- versus co-diffusion).

the biofilm was measured directly from the image projection with a reported resolution of 10 μm. Our imaging approach is similar but its implementation is faster and more automated. Moreover, even with a low-power stereomicroscope, a higher resolution (e.g., few microns thick biofilms or individual cell dimensions) can be obtained depending on the objective and camera specifications (Milferstedt *et al.* 2009). Also, biofilm imaging contrast problems may be addressed more effectively by complementing with transmitted darkfield illumination.

In a stereomicroscope the two separate optical paths arrangement produce a 3D visualization of the sample being examined. However, to consider the 3D structure, a reconstructed composite image of the biofilm structure may be obtained by taking pictures at different axial planes corresponding to various membrane cross-sections, or by rotating the membrane. Biofilm 3D intact structure may be also obtained using more elaborated techniques, such as optical coherence tomography (Wagner *et al.* 2010) and magnetic resonance imaging (Manz *et al.* 2003). A micro-scale CLSM 3D analysis of biofilms growing on membranes and considering the curvature of the attachment surface has also been developed (Bjørkøy & Fiksdal 2009). However, all these approaches are time consuming and require more sophisticated equipment.

Substrate conversion and model simulations

Using the imaging data, the experimental profiled biofilm sections were reproduced in MATLAB and COMSOL. Fluid dynamics and substrate transport and reaction were solved with the model, and total substrate conversion rates per projected area were calculated. At higher flow velocities, microbial activity showed a significant increase within the biofilms (Figure 4(b)). Concentration profiles showed the biofilm substrate-limited areas and counter-diffusion (Figures 4(c) and 4(d)). A comparison between experimental conversion rates and simulation results in the studied sections showed small differences of about 10% in the substrate conversion, referenced to the projected membrane area, for $u = 0.001$ ($\mathrm{Re} = 1.7$) and $u = 0.005$ m/s ($\mathrm{Re} = 8.5$) (Figure 5(a)). Higher differences of 15–30% were observed for $u = 0.025$ ($\mathrm{Re} = 42$) and $u = 0.1$ m/s ($\mathrm{Re} = 168$). At these increased flow velocities, total substrate conversion was higher in the biofilms with higher roughness.

The observed trends were similar between experimental and modelling results. These results showed the potential to use the theoretical model to evaluate biofilm overall substrate utilization related to biofilm heterogeneity. Differences may have resulted from considering a reference density, and typical kinetic and effective diffusivity parameters, as well as neglecting advection within the biofilm. While advective solute transport inside biofilms has been shown to be negligible at the tested range of fluid velocities (Stewart 2012), biofilm density and porosity may affect activity and substrate transport.

We assumed the biofilm subdomain was rigid, whereas biofilms can exhibit viscoelastic behaviour under longer timescales (Klapper & Dockery 2010). Since our imaging and microsensor profiles were carried out under short timescales (minutes) and relatively low shear, viscoelastic deformation during the imaging or profiles is unlikely to have been significant. Deformation and detachment could lead to filamentous structures (e.g., streamers), which can significantly enhance external mass transfer (Taherzadeh *et al.* 2012). However, our experimental biofilm structures had no detectable oscillating heterogeneities at the conditions tested.

Effect of flow velocity on substrate conversion in rough biofilms

The experimental and modelling results were used to assess the effect of flow velocities on substrate fluxes in biofilms with similar average thicknesses and biomass (similar areas), but very different roughnesses. Conversion rates increased with velocity in both cases as expected (Figure 5(a)). At higher velocities the external resistance to mass transfer decreases; the mass transfer boundary layer becomes thinner and convection becomes more important (Picioreanu *et al.* 2000). At low flow velocities conversion rates were lower in the rougher biofilm structure (Figure 5). Previous studies of co-diffusional biofilms showed that higher roughness typically results in lower overall substrate fluxes, especially for laminar flow (Picioreanu *et al.* 2000). Interestingly in our results, which are under substrate counter-diffusion, increasing velocity ($u = 0.025$ (Re = 42) and 0.1 m/s (Re = 168)) led to higher overall substrate transformation rates with higher roughnesses. Simulated activity profiles showed that with increased velocity and heterogeneity there was an apparent higher effective active biofilm area (Figures 5 and 4(b)). The heterogeneous biofilm supports higher conversion rates through increased biofilm surface area.

To further study substrate conversion, we also simulated the studied structures under co-diffusion at similar substrate loadings. Higher substrate conversion was observed under counter-diffusion for the studied velocity range, particularly for lower flow velocities (Figure 5(b)). The counter-diffusional substrate rate-limitation within the biofilm was negligible (as example see Figures 4(b)–4(d)). At lower flow velocity, diffusional limitation from the bulk increases due to the greater boundary layer thickness. This affects both electron donor and acceptor substrates in a co-diffusion biofilm; however, it only affects the externally supplied substrate in a counter-diffusional biofilm, which explains the higher substrate conversion rates for low velocities.

As mentioned before for laminar flow, increased roughness decreased substrate uptake under co-diffusion. However, we observed an increase in conversion when comparing a very rough with a moderately heterogeneous structure at $u = 0.1$ m/s. We ran the simulations also at $u =$ 0.25 m/s (Re = 420) to confirm this trend (Figure 5(b)). This may be due to the formation of more convective recirculation regions that increase mass transfer (Picioreanu *et al.* 2000).

These preliminary results suggest that for similar substrate conditions and flow regime, in counter-diffusional biofilms higher substrate fluxes can be sustained in heterogeneous structures than in conventional biofilms. This study also shows that the effect of biofilm roughness on conversion rates in counter- and co-diffusional biofilms can be different.

CONCLUSIONS

A combined experimental and modelling approach for studying biofilm substrate conversion rates was developed and tested using conditions found in biofilm reactor applications. Our modelling results were consistent with experimental observations. These results highlight the potential to use a simple *in situ* image acquisition and processing approach coupled to a simplified theoretical model, to evaluate biofilm overall substrate utilization related to structural heterogeneity, and to obtain approximate estimations of conversion rates. The presented imaging method is relatively fast and the model computationally easy to implement. This approach may allow a systematic study of biofilm development in MBfRs related to fluid dynamics, including structural heterogeneity and detachment. Also biofilm kinetic and substrate mass transport parameters may be estimated by comparing experimental and modelling results. Using images taken from different directions for the same section may extend the method to a 3D representation of the biofilm structure. Particularly, the extent of the effect of surface heterogeneity on substrate conversion in counter-diffusional biofilms should be studied further.

ACKNOWLEDGEMENTS

This research was supported by a CAREER Award to Robert Nerenberg (National Science Foundation grant No. CBET-0954918), and the Bayer Predoctoral Research Fellowship from the Bayer Foundation and the Center for Environmental Science and Technology (CEST) at the University of Notre Dame. We gratefully acknowledge computational resources provided by the University of Notre Dame Center for Research Computing (CRC).

REFERENCES

Ahmed, T., Semmens, M. J. & Voss, M. A. 2004 Oxygen transfer characteristics of hollow-fiber, composite membranes. *Advances in Environmental Research* **8** (3), 637–646.

Alpkvist, E., Picioreanu, C., van Loosdrecht, M. C. M. & Heyden, A. 2006 Three-dimensional biofilm model with individual cells and continuum EPS matrix. *Biotechnology and Bioengineering* **94** (5), 961–979.

Bae, W. & Rittmann, B. E. 2000 A structured model of dual-limitation kinetics. *Biotechnology and Bioengineering* **49** (6), 683–689.

Bjørkøy, A. & Fiksdal, L. 2009 Characterization of biofouling on hollow fiber membranes using confocal laser scanning microscopy and image analysis. *Desalination* **245** (1), 474–484.

De Beer, D., Stoodley, P., Roe, F. & Lewandowski, Z. 1994 Effects of biofilm structures on oxygen distribution and mass transport. *Biotechnology and Bioengineering* **43** (11), 1131–1138.

Dos Santos, L. & Livingston, A. 1995 Membrane-attached biofilms for VOC wastewater treatment I: Novel in situ biofilm thickness measurement technique. *Biotechnology and Bioengineering* **47** (1), 82–89.

Downing, L. S. & Nerenberg, R. 2008a Effect of bulk liquid BOD concentration on activity and microbial community structure of a nitrifying, membrane-aerated biofilm. *Applied Microbiology and Biotechnology* **81** (1), 153–162.

Downing, L. S. & Nerenberg, R. 2008b Effect of oxygen gradients on the activity and microbial community structure of a nitrifying, membrane-aerated biofilm. *Biotechnology and Bioengineering* **101** (6), 1193–1204.

Eberl, H. J., Picioreanu, C., Heijnen, J. J. & van Loosdrecht, M. C. M. 2000 A three-dimensional numerical study on the correlation of spatial structure, hydrodynamic conditions, and mass transfer and conversion in biofilms. *Chemical Engineering Science* **55** (24), 6209–6222.

Heydorn, A., Nielsen, A. T., Hentzer, M., Sternberg, C., Givskov, M., Ersbøll, B. K. & Molin, S. 2000 Quantification of biofilm structures by the novel computer program COMSTAT. *Microbiology* **146** (10), 2395–2407.

Klapper, I. & Dockery, J. 2010 Mathematical description of microbial biofilms. *SIAM Review* **52** (2), 221–265.

Lewandowski, Z. & Beyenal, H. 2007 *Fundamentals of Biofilm Research*. CRC Press, Boca Raton, FL, USA.

Manz, B., Volke, F., Goll, D. & Horn, H. 2003 Measuring local flow velocities and biofilm structure in biofilm systems with magnetic resonance imaging (MRI). *Biotechnology and Bioengineering* **84** (4), 424–432.

Martin, K. J. & Nerenberg, R. 2012 The membrane biofilm reactor (MBfR) for water and wastewater treatment: principles, applications, and recent developments. *Bioresource Technology* **122**, 83–94.

Martin, K. J., Picioreanu, C. & Nerenberg, R. 2013 Multidimensional modeling of biofilm development and fluid dynamics in a hydrogen-based, membrane biofilm reactor (MBfR). *Water Research* **47** (13), 4739–4751.

Milferstedt, K., Pons, M. N. & Morgenroth, E. 2009 Analyzing characteristic length scales in biofilm structures. *Biotechnology and Bioengineering* **102** (2), 368–379.

Picioreanu, C., van Loosdrecht, M. C. M. & Heijnen, J. J. 2000 A theoretical study on the effect of surface roughness on mass transport and transformation in biofilms. *Biotechnology and Bioengineering* **68** (4), 355–369.

Rittmann, B. E. & McCarty, P. L. 2001 *Environmental Biotechnology: Principles and Applications*. McGraw-Hill, Boston, MA, USA.

Rittmann, B. E., Pettis, M., Reeves, H. W. & Stahl, D. A. 1999 How biofilm clusters affect substrate flux and ecological selection. *Water Science and Technology* **39** (7), 99–105.

Semmens, M. J. & Essila, N. J. 2001 Modeling biofilms on gas-permeable supports: flux limitations. *Journal of Environmental Engineering* **127** (2), 126–133.

Stewart, P. S. 2003 Diffusion in biofilms. *Journal of Bacteriology* **185** (5), 1485–1491.

Stewart, P. S. 2012 Mini-review: convection around biofilms. *Biofouling* **28** (2), 187–198.

Taherzadeh, D., Picioreanu, C. & Horn, H. 2012 Mass transfer enhancement in moving biofilm structures. *Biophysical Journal* **102** (7), 1483–1492.

Terada, A., Lackner, S., Tsuneda, S. & Smets, B. F. 2007 Redox-stratification controlled biofilm (ReSCoBi) for completely autotrophic nitrogen removal: the effect of co versus counter-diffusion on reactor performance. *Biotechnology and Bioengineering* **97** (1), 40–51.

Wagner, M., Taherzadeh, D., Haisch, C. & Horn, H. 2010 Investigation of the mesoscale structure and volumetric features of biofilms using optical coherence tomography. *Biotechnology and Bioengineering* **107** (5), 844–853.

Wanner, O., Eberl, H., Morgenroth, E., Noguera, D., Picioreanu, C., Rittmann, B. & van Loosdrecht, M. 2006 *Mathematical Modeling of Biofilms*. Scientific and Technical Report No. 18. IWA Publishing, London.

Yang, X., Beyenal, H., Harkin, G. & Lewandowski, Z. 2000 Quantifying biofilm structure using image analysis. *Journal of Microbiological Methods* **39** (2), 109–119.

First received 10 September 2013; accepted in revised form 14 February 2014. Available online 3 March 2014